REPORT NO.
UCB/SEMM-95/04

STRUCTURAL ENGINEERING
MECHANICS AND MATERIALS

ADVANCES IN DOUBLET MECHANICS: II. FREE BOUNDARY REFLECTION OF P- AND S- WAVES IN GRANULAR MEDIA

BY

M. ZHANG
AND
M. FERRARI

JUNE 1995

DEPARTMENT OF CIVIL ENGINEERING
UNIVERSITY OF CALIFORNIA
BERKELEY, CALIFORNIA

Advances in Doublet Mechanics

II. Free Boundary Reflection of P- and S-Waves in Granular Media

Miqin Zhang[1], Mauro Ferrari[1,2]

[1] Department of Materials Science and Mineral Engineering, University of California, Berkeley. CA 94720, USA

[2] Department of Civil Engineering, University of California, Berkeley, CA 94720, USA

The free-boundary reflection of plane waves propagating in macroscopically isotropic granular arrays is studied using the methods of doublet elasticity. The effects of granule size on the reflection characteristics of P- and S-waves of given wavelength are established. It is shown that the critical angles of mode conversion, the phase changes, and the amplitude ratios are scale-related. The classical reflection results of continuum elastodynamics are retrieved in the non-scale and infinite wavelength limits.

Introduction

Microscopically isotropic, infinite plane regular assemblies of discrete nodes capable of elastic axial interactions were shown (Granik and Ferrari, 1995) to sustain both longitudinal and shear vertical plane waves for all values of the dimensionless scaling parameter $l=\lambda/\eta$, where λ is the wavelength and η is the internodal distance, or granule dimension. Ibidem, it was also shown that the incorporation of scaling effects permits the modelling of physical observations that are otherwise intractable in terms of a general theory. Among these are the phenomena of dispersion and retardation of both P- and S- waves, which are incompatible with homogeneous continuum linear elasticity, but are successfully predicted employing the microstructure-accounting methods of multi-scale Doublet Mechanics (DM).

In the first part (Granik and Ferrari, 1995) of this sequence of coordinated papers, the elastodynamic study was limited to infinite media, and in this memoir we extend their work, by considering the problem of reflection of plane waves at the free surface of macroscopically isotropic granular media. While the problem of plane elastodynamics in granular media has received considerable attention in the literature (see discussion in Granik and Ferrari, 1995), the issue of wave reflection has, to the best of the authors' knowledge, never been addressed.

The methods employed in this paper are again those of multi-scale Doublet Mechanics. In order to make the paper self-contained, the necessary basic equations of Doublet Mechanics are summarized in the next section. For a detailed presentation of theory, however, the reader

is referred to the first part(Granik and Ferrari, 1995) of this sequence and references therein. Notation throughout this sequence is also coordinated with (Granik and Ferrari, 1995).

In the first part of this paper, the non-scale version of the problem of plane wave reflection is considered, with results that are in compliance with those of continuum linear elastodynamics. However, in later sections it is demonstrated that the simplest scaling variable of the theory elicits results that are qualitatively different from the classical ones. In particular, it is found that the critical angles of mode conversion, the phase changes and the amplitude ratios are dependent on the dimensionless scaling parameter, and thus on granule size for a fixed wavelength. The dependence is more pronounced at shorter wavelengths.

The analysis in what follows is, for mathematical simplification and physical explicitness, based on a set of assumptions: (i) no body forces are acting on the granular domain; (ii) the doublets are capable of axial microstresses only; (iii) the doublet constitutive response is linear elastic and local, with microstresses in the α-th doublet depending on the α-th microstrain only; (iv) the granular packing is macroscopically isotropic in the plane of propagation.

It is noted that (iv) is satisfied by choosing the plane of propagation to be the basal plane of the cubic-tetrahedral packing, which is elastically isotropic in the nonscale (macroscopic) limit, but becomes anisotropic once scaling effects are accounted for (Granik and Ferrari, 1995).

In this paper, the first and fundamental scale-accounting version of the Doublet-Mechanical approach is employed, corresponding to the truncation of the displacement expansion at M=2 in equation (1). This choice retains the advantage of analytic treatment, while sufficing to establish the above-mentioned qualitative features of the scale-accounting treatment. The presently employed methods of analysis are not confined to the specific packing here discussed, but are applicable to any other granular array of interest.

Preliminaries on Doublet Mechanics

In Doublet Mechanics, granular bodies are represented as assemblies of discrete nodes arranged with translational periodicity. Any pair of such nodes is called a doublet. Let $\Re$ be the region occupied by the granular media in the reference configuration. All the vector and tensor variables and quantities are defined with respect to a rectangular Cartesian frame of reference x_i with $\mathbf{i}_i$ as its unit vector. Plane granular assemblies are assumed, so the subscript takes on values 1 and 2. The summation convention is enforced in the same range on Latin subscripts, but not on superscripts. Greek subscripts refer to doublet numbers.

Following the above-mentioned coordinate system configuration, the increment of the displacement vector $\mathbf{u}(\mathbf{x})$, $\mathbf{x} \in \Re$, in the α-th doublet may be expressed in a convergent Taylor series as (Granik and Ferrari, 1993)

$$\Delta\vec{u}_\alpha=\sum_{x=1}^{M}\frac{\eta_\alpha{}^x}{x!}(\vec{\tau}_\alpha\cdot\vec{\nabla})^x\vec{u}(\vec{x},t) \tag{1}$$

where ∇ is the Hamilton operator and "$\cdot$" denotes the dot product; the subscript α denotes the particular doublet under consideration; η_α are the corresponding doublet length and τ_α are the unit doublet vectors in the reference configurations; and M indicates the degree of approximation. The theory is multi-scale in nature, since M may be taken to be any positive integer. For simplicity, in this article, only the cases of M=1(non-scaling, the first degree approximation) and M=2(scaling, the second degree approximation) are considered.

The kinematic equations that relate the doublet microstrains of elongation ε_α of the α-th doublet to the vector fields of the granule translations **u** are defined as (Granik and Ferrari, 1993)

$$\varepsilon_\alpha=\tau_{\alpha i}\sum_{x=1}^{M}\frac{(\eta_\alpha)^{x-1}}{x!}\tau_{\alpha k_1}\ldots\tau_{\alpha k_x}\frac{\partial^x(u_i)}{\partial x_{k_1}\ldots\partial x_{k_x}} \tag{2}$$

where $\tau_{\alpha i}$ are the cartesian components of vectors of τ_α. Via assumption (iii) of the introduction, the constitutive equation that relates the axial microstresses P_α with the microstrains can be defined as (Granik and Ferrari, 1993)

$$P_\alpha=C\varepsilon_\alpha \tag{3}$$

where C is a constant.

The traction vector T_i acting on the boundary S of the granular assembly is given by

$$T_i = n_{k_1} \sum_{\alpha=1}^{n} \tau_{\alpha i} \tau_{\alpha k_1} \sum_{x=1}^{M} (-1)^x \frac{(\eta_\alpha)^{x-1}}{x!} \tau_{\alpha k_2} \ldots \tau_{\alpha k_x} \frac{\partial^{x-1}(-P_\alpha)}{\partial x_{k_2} \ldots \partial x_{k_x}} \tag{4}$$

where n_{k_1} denotes the outward unit normal to S. By comparison with the Cauchy relationship

$$T_i = \sigma_{ki} n_k \tag{5}$$

where σ_{ki} is the stress tensor, it follows that the macroscopic stress tensor is expressed, in the M-th order approximation, as

$$\sigma_{k_1 i}^{(M)} = \sum_{\alpha=1}^{n} \tau_{\alpha i} \tau_{\alpha k_1} \sum_{x=1}^{M} (-1)^x \frac{(\eta_\alpha)^{x-1}}{x!} \tau_{\alpha k_2} \ldots \tau_{\alpha k_x} \frac{\partial^{x-1}(-P_\alpha)}{\partial x_{k_2} \ldots \partial x_{k_x}} \tag{6}$$

This establishes a scale-dependent relationship between the M-th order approximation to the stress tensor, the microstresses and the microstructural variables. The stress relation (6) may also be expressed in terms of displacements, by substitution from constitutive equation (3) and kinematic equation (2).

Model and Formulation of Reflection of Incident waves

In this study, we consider single-frequency time-harmonic waves only. Figure 1 sketches a plane P-wave travelling at an incident angle θ_0 . Upon impact with the free surface x_2=0, this wave gives rise to a reflected P-wave and a reflected S- wave, with reflection angles θ_1 and θ_2 , respectively.

The incident and reflected waves propagating in the half-space x_2<0 are defined by the following equations

$$\vec{u}^{(n)}=A_n\vec{d}^{(n)}\exp(i\eta^{(n)}) \tag{7}$$

where

$$\eta^{(n)}=k_n(\vec{x}\cdot\vec{p}^{(n)}-c_n t) \tag{8}$$

where A_n are the amplitudes of the waves and $\mathbf{d}^{(n)}$, the unit vectors of particle motion; $\mathbf{x}$ is the position vector and $\mathbf{p}^{(n)}$, the unit vectors of propagation; k_n are the wave numbers and c_n are the phase velocities of wave propagation. The index n is assigned the value of 0 for the incident P- wave, 1 for reflected P-wave and 2 for reflected S-waves.

From the geometry of Figure 1 we have, for the incident P-wave

$$\vec{d}^{(0)}=\vec{p}^{(0)}, \quad c_0=c_L \tag{9}$$

$$\vec{p}^{(0)}=\sin\theta_0 i_1+\cos\theta_0 i_2 \tag{10}$$

$$\vec{u}^{(0)}=\begin{bmatrix}u_1^{(0)}\\u_2^{(0)}\end{bmatrix}=\begin{bmatrix}A_0\sin\theta_0\exp[ik_0(x_1\sin\theta_0+x_2\cos\theta_0-c_0t)]\\A_0\cos\theta_0\exp[ik_0(x_1\sin\theta_0+x_2\cos\theta_0-c_0t)]\end{bmatrix}; \tag{11}$$

for an incident S-wave

$$\vec{d}^{(0)}=i_3\times\vec{p}^{(0)},\quad c_0=c_T \tag{12}$$

$$\vec{p}^{(0)}=\sin\theta_0 i_1+\cos\theta_0 i_2 \tag{13}$$

$$\vec{d}^{(0)}=-\cos\theta_0 i_1+\sin\theta_0 i_2 \tag{14}$$

$$\vec{u}^{(0)}=\begin{bmatrix}u_1^{(0)}\\u_2^{(0)}\end{bmatrix}=\begin{bmatrix}-A_0\cos\theta_0\exp([ik_0(x_1\sin\theta_0+x_0\cos\theta_0-c_0t)]\\A_0\sin\theta_0\exp[ik_0(x_1\sin\theta_0+x_2\cos\theta_0-c_0t)]\end{bmatrix}; \tag{15}$$

for the reflected P-wave

$$\vec{p}^{(1)}=\sin\theta_1 i_1-\cos\theta_1 i_2 \tag{16}$$

$$\vec{d}^{(1)}=\vec{p}^{(1)},\quad c_1=c_L \tag{17}$$

$$\vec{u}^{(1)}=\begin{bmatrix}u_1^{(1)}\\u_2^{(1)}\end{bmatrix}=\begin{bmatrix}A_1\sin\theta_1\exp([ik_1(x_1\sin\theta_1-x_2\cos\theta_1-c_1t)]\\-A_1\cos\theta_1\exp[ik_1(x_1\sin\theta_1-x_2\cos\theta_1-c_1t)]\end{bmatrix}; \tag{18}$$

and finally for the reflected S- wave

$$\vec{p}^{(2)}=\sin\theta_2 i_1-\cos\theta_2 i_2 \tag{19}$$

$$\vec{d}^{(2)}=i_3\times\vec{p}^{(2)}, \qquad c_2=c_T \tag{20}$$

$$\vec{d}^{(2)}=\cos\theta_2 i_1+\sin\theta_2 i_2 \tag{21}$$

$$\vec{u}^{(2)}=\begin{bmatrix}u_1^{(2)}\\u_2^{(2)}\end{bmatrix}=\begin{bmatrix}A_2\cos\theta_2\exp[ik_2(x_1\sin\theta_2-x_2\cos\theta_2-c_2t)]\\A_2\sin\theta_2\exp[ik_2(x_1\sin\theta_2-x_2\cos\theta_2-c_2t)]\end{bmatrix}. \tag{22}$$

In the above, c_L and c_T are the propagation velocities of P- and S- waves respectively. The derivatives of the displacement of the incident P-wave are

$$\frac{\partial u_1^{(0)}}{\partial x_1}=iA_0k_0\sin^2(\theta_0)\exp(i\eta^{(0)}),\qquad \frac{\partial u_1^{(0)}}{\partial x_2}=iA_0k_0\sin(\theta_0)\cos(\theta_0)\exp(i\eta^{(0)})$$

$$\frac{\partial u_2^{(0)}}{\partial x_1}=iA_0k_0\cos(\theta_0)\sin(\theta_0)\exp(i\eta^{(0)}),\qquad \frac{\partial u_2^{(0)}}{\partial x_2}=iA_0k_0\cos^2(\theta_0)\exp(i\eta^{(0)})$$

$$\frac{\partial^2 u_1^{(0)}}{\partial x_1^2}=-A_0k_0^2\sin^3(\theta_0)\exp(i\eta^{(0)}),\qquad \frac{\partial^2 u_1^{(0)}}{\partial x_2^2}=-A_0k_0^2\sin(\theta_0)\cos^2(\theta_0)\exp(i\eta^{(0)}) \tag{23}$$

$$\frac{\partial^2 u_2^{(0)}}{\partial x_1^2}=-A_0k_0^2\sin^2(\theta_0)\cos(\theta_0)\exp(i\eta^{(0)}),\qquad \frac{\partial^2 u_2^{(0)}}{\partial x_2^2}=-A_0k_0^2\cos^3(\theta_0)\exp(i\eta^{(0)})$$

$$\frac{\partial^2 u_2^{(0)}}{\partial x_1x_2}=-A_0k_0^2\sin(\theta_0)\cos^2(\theta_0)\exp(i\eta^{(0)}),\qquad \frac{\partial^2 u_1^{(0)}}{\partial x_1x_2}=-A_0k_0^2\sin^2\theta_0\cos(\theta_0)\exp(i\eta^{(0)})$$

Derivatives for the other waves are similarly defined.

Via (6) the free stress boundary conditions at plane $x_2=0$ may be expressed as

$$\sum_n \sigma_{21}^{(n)}=0, \tag{24}$$

$$\sum_n \sigma_{22}^{(n)}=0 \tag{25}$$

where the summation is performed over each wave n, and the superscript M is dropped for notational conventional convenience.

In analogy with continuum elastodynamics(Achenbach, 1973), for a given incident wave, the amplitudes, the unit propagation vectors, and the wavenumber must be computed from the boundary conditions. Thus the problem is reduced to solving for the amplitude coefficients and reflection angles of reflected waves, on the basis of the above stated stress free boundary conditions. This approach also allows us to develop families of solutions to the reflection of incident waves for various boundary conditions. Some scaling and non-scaling reflection problems are studied next.

Case I. Reflection of an incident P-wave in non-scale analysis(M=1) with doublet axis τ_3 parallel to x_1 axis

According to the coordinate system defined in Figure 1, we can write the direction matrix of doublets as follows

$$\begin{bmatrix} \tau_{11} & \tau_{12} \\ \tau_{21} & \tau_{22} \\ \tau_{31} & \tau_{32} \end{bmatrix} = \begin{bmatrix} -\cos\phi & -\sin\phi \\ \cos\phi & -\sin\phi \\ 1 & 0 \end{bmatrix} \tag{26}$$

where ϕ is 60^0 for the basal plane of the cubic tetrahedral packing. For the non-scaling case (M=1) this plane is elastically isotropic (Granik and Ferrari, 1995).

The stress relation (6) for M=1 is thus reduced to

$$\sigma_{ji}=\sum_{\alpha=1}^{3}\tau_{\alpha i}\tau_{\alpha j}P_{\alpha} \tag{27}$$

where, for plane waves, i, j=1,2. From the boundary condition(24), (25), constitutive relation (3), and kinematic equation(2), we obtain the following relations between the incident and reflected waves

$$A_0k_0[\sin^2\theta_0+3\cos^2\theta_0]\exp(i\eta^{(0)})+A_1k_1[\sin^2\theta_1+3\cos^2\theta_1]\exp(i\eta^{(1)})-A_2k_2\sin(2\theta_2)\exp(i\eta^{(2)})=0 \tag{28}$$

$$A_0k_0\sin(2\theta_0)\exp(i\eta^{(0)})-A_1k_1\sin(2\theta_1)\exp(i\eta^{(1)}1)-A_2k_2\cos(2\theta_2)\exp(i\eta^{(2)})=0. \tag{29}$$

Since equations (28)and (29) are valid for all values of x_1 and t at $x_2=0$, the existence of solutions of the set of equations requires that the exponential must appear as factors in both equations(Achenbach, 1973). This will be satisfied only when

$$\eta^0=\eta^1=\eta^2 \tag{30}$$

We conclude, from inspection of the definition of $\eta^{(n)}$ in (8), that

$$k_0\sin\theta_0=k_1\sin\theta_1=k_2\sin\theta_2=\kappa \tag{31}$$

$$k_0 c_L = k_1 c_L = k_2 c_T = \omega \tag{32}$$

From (31) and (32), it follows

$$\theta_0 = \theta_1, \quad \theta_2 = \arcsin(\kappa^{-1} \sin\theta_0) \tag{33}$$

$$k_1 = k_0, \qquad \frac{k_2}{k_0} = \frac{c_L}{c_T} = \kappa. \tag{34}$$

By employing (33) and (34), the algebraic equations for the amplitude ratios A_1/A_0 and A_2/A_0 are obtained from (28) and (29):

$$\frac{A_1}{A_0}(\sin^2\theta_0 + 3\cos^2\theta_0) - \frac{A_2}{A_0}\kappa \sin 2\theta_2 = -(\sin^2\theta_0 + 3\cos^2\theta_0) \tag{35}$$

$$\frac{A_1}{A_0}\sin 2\theta_0 + \frac{A_2}{A_0}\kappa \cos 2\theta_2 = \sin 2\theta_0. \tag{36}$$

A typical plot of amplitude ratios A_1/A_0 , A_2/A_0 versus the angle of incidence is shown in Figure 2 for the standard value of material constant $\kappa = 3^{1/2}$(Kolsky, 1963). This value of the material constant κ was chosen for ease of comparison with literature results. It is found that the results obtained using DM theory in the first degree approximation (M=1, non-

scaling) corresponds exactly to those of classical continuum elasticity(Kolsky, 1963; Achenbach, 1973).

It is observed from Figure 2 that: (i) for normal incidence (θ_0=0), the amplitude of the reflected S wave is zero, the incident P-wave is reflected as a P-wave only, and the amplitude of the wave is equal to that of the incident wave with a phase change of π; (ii) for an angle of incidence about 45^0, the amplitude of the reflected S wave reaches the maximum, which is greater than that of the incident wave; (iii) for the angles of incidence $\theta_0=60^0$ and about 80^0, the incident P-wave is reflected as a S-wave only, which is known as mode conversion phenomena; (iv) for $\theta_0=90^0$, the reflected S wave vanishes and the incident P-wave is again reflected as a P-wave; (v) the reflected P-wave have same phase as the incident P-wave between about 60^0-80^0, and otherwise it is 180^0 out of phase to the incident wave.

Case II. Reflection of incident P-wave in non-scaling analysis(M=1) for doublet axis τ_3 at an angle of γ with respect to x_1 axis

The geometry of this case is sketched in Figure 3, and the direction matrix of the rotation may be written as

$$\tau_{ij}=\begin{bmatrix}\tau_{11} & \tau_{12}\\ \tau_{21} & \tau_{22}\\ \tau_{31} & \tau_{32}\end{bmatrix}=\begin{bmatrix}-\cos(\phi-\gamma) & -\sin(\phi-\gamma)\\ \cos(\phi+\gamma) & -\sin(\phi+\gamma)\\ \cos\gamma & -\sin\gamma\end{bmatrix}. \qquad (37)$$

By (2) and (3), the stress relation (6) may be expressed in terms of the components of displacement as

$$\sigma_{21}^{(n)}=\sum_{n}\sum_{\alpha=1}^{3}(\tau_{\alpha 2}\tau_{\alpha 1}^{3}\frac{\partial u_1^{(n)}}{\partial x_1}+\tau_{\alpha 1}^{2}\tau_{\alpha 2}^{2}(\frac{\partial u_2^{(n)}}{\partial x_1}+\frac{\partial u_1^{(n)}}{\partial x_2})+\tau_{\alpha 1}\tau_{\alpha 2}^{3}\frac{\partial u_2^{(n)}}{\partial x_2}) \tag{38}$$

$$\sigma_{22}^{(n)}=\sum_{n}\sum_{\alpha=1}^{3}(\tau_{\alpha 2}^{2}\tau_{\alpha 1}^{2}\frac{\partial u_1^{(n)}}{\partial x_1}+\tau_{\alpha 1}\tau_{\alpha 2}^{3}(\frac{\partial u_1^{(n)}}{\partial x_2}+\frac{\partial u_2^{(n)}}{\partial x_1})+\tau_{\alpha 2}^{4}\frac{\partial u_2^{(n)}}{\partial x_2}) \ . \tag{39}$$

Substituting (38) and (39) into (24), (25), and following the same procedure as case I, it is proven that the angle of reflected P-wave is equal to the angle of incident P-wave and the angle of reflected S wave still satisfies (33). The amplitude ratio expressions can thus be reduced to

$$\begin{aligned}&\sum_{\alpha}\tau_{\alpha 2}\tau_{\alpha 1}^{3}(A_0k_0\sin^2\theta_0+A_1k_1\sin^2\theta_1+A_2k_2\cos\theta_2\sin\theta_2)\\+&\sum_{\alpha}\tau_{\alpha 1}^{2}\tau_{\alpha 2}^{2}(A_0k_0\sin 2\theta_0-A_1k_1\sin 2\theta_1-A_2k_2\cos^2\theta_2+A_2k_2\sin^2\theta_2)\\+&\sum_{\alpha}\tau_{\alpha 2}^{3}\tau_{\alpha 1}(A_0k_0\cos^2\theta_0+A_1k_1\cos^2\theta_1-\frac{1}{2}A_2k_2\sin 2\theta_2)=0.\end{aligned} \tag{40}$$

$$\sum_{\alpha} \tau_{\alpha 2}^2 \tau_{\alpha 1}^2 (A_0 k_0 \sin^2\theta_0 + A_1 k_1 \sin^2\theta_1 + \frac{1}{2} A_2 k_2 \sin 2\theta_2)$$
$$+\sum_{\alpha} \tau_{\alpha 1} \tau_{\alpha 2}^3 (A_0 k_0 sin2\theta_0 - A_1 k_1 \sin 2\theta_1 - A_2 k_2 \cos^2\theta_2 + A_2 k_2 \sin^2\theta_2) \qquad (41)$$
$$\sum_{\alpha} \tau_{\alpha 2}^4 (A_0 k_0 \cos^2\theta_0 + A_1 k_1 \cos^2\theta_1 - \frac{1}{2} A_2 k_2 \sin 2\theta_2) = 0.$$

The ratios of the amplitudes of the reflected waves to the amplitude of the incident P-wave have been plotted for varying angle of γ and it was found that the reflection coefficients are independent of the rotation angle of γ and the dependence of amplitudes of reflected waves on the incident angles is exactly the same as in case 1.

Case III. Reflection of incident P-wave in scale-accounting analysis (M=2) with Doublet axis τ_3 parallel to x_1

The first order scale-accounting case is addressed next, by choosing the order of approximation M=2. Referring to the (2) and (6), the stress relations may be reduced to

$$\sigma_{ji} = C \sum_{\alpha} \tau_{\alpha j} (\tau_{\alpha i} \varepsilon_{\alpha} - \frac{\eta_{\alpha}}{2} \tau_{\alpha k} \tau_{\alpha i} \frac{\partial \varepsilon_{\alpha}}{\partial x_k}) \qquad (42)$$

In this case, unlike the case of M=1 in which the stresses are the function of strain only,

the stresses are the function of both strains and the derivatives of strains. Following the same steps as the Case I, by employing the stress-strain relation (42) and the stress free boundary condition (24) and (25), the following relations are derived

$$\theta_1=\theta_0, \quad k_1=k_0 \tag{43}$$

$$\theta_2=\arcsin(\kappa^{-1}\sin\theta_0) \tag{44}$$

where $\kappa=k_2/k_0$.

With (43) and (44) and the stress free boundary conditions (24) and (25), the algebraic equations for amplitude ratios of incident and reflected waves A_1/A_0 and A_2/A_0 can be expressed as the following,

$$\begin{aligned}
&\left[\frac{3}{4}\sin\theta_0\cos\theta_0-i\frac{\sqrt{3}}{16}\frac{\pi}{l}\sin\theta_0-i\frac{11}{16}\sqrt{3}\frac{\pi}{l}\sin\theta_0\cos^2\theta_0\right]\frac{A_1}{A_0}\\
&+\left[\frac{\sqrt{3}}{8}+\frac{\sqrt{3}}{4}\cos^2\theta_0+i\frac{5}{16}\frac{\pi}{l}\sqrt{2+\cos^2\theta_0}-i\frac{5}{16}\frac{\pi}{l}\sqrt{2+\cos^2\theta_0}\cos^2\theta_0\right]\frac{A_2}{A_0}\\
&=\frac{3}{4}\sin\theta_0\cos\theta_0+i\frac{\sqrt{3}}{16}\frac{\pi}{l}\sin\theta_0+i\frac{\sqrt{3}}{2}\frac{\pi}{l}\sin\theta_0\cos^2\theta_0
\end{aligned} \tag{45}$$

$$[-\frac{3}{8}-\frac{3}{4}\cos^2\theta_0+i\frac{9}{16}\sqrt{3}\frac{\pi}{l}\cos\theta_0]\frac{A_1}{A_0}+[\frac{1}{4}\sqrt{6+3\cos^2\theta_0}\sin\theta_0-i\frac{9}{16}\frac{\pi}{l}\sin\theta_0]\frac{A_2}{A_0} \tag{46}$$
$$=\frac{3}{8}+\frac{3}{4}\cos^2\theta_0+i\frac{9}{16}\frac{\pi}{l}\sqrt{3}\cos\theta_0$$

The ratios A_1/A_0 and A_2/A_0 versus incident angles are plotted in Figures 4 and 5 for different values of scaling factors $l = \lambda/\eta_\alpha$, where λ is the wave length and η_α is the central distance of doublets as shown in Figure 1. For $l=\infty$, the non-scaling results of case I are retrieved. In the figures throughout the paper, the following nomenclature is employed for the axis labels: the letter(s) before the dash line indicates the types of incident wave and the letter(s) after the dash line indicates the types of reflected waves. For instance, a reflected P-wave due to the incident S wave is identified as S-P-wave.

From Figures 4 and 5, it is observed that: (i) the amplitudes of the reflected waves not only depend on the incident angle and material property κ as in the non-scaling case, but also depend on the scaling factor l, which reflects the size of the doublet; the dependence is especially strong at the wavelength comparable to the particle size. (ii) For incident angle $\theta_0=0$, the reflected S-wave vanishes and incident P-wave is reflected as a P-wave; and the magnitude of amplitude of reflected P-wave decrease sharply with l. (iii) At grazing incidence ($\theta_0=90^0$), no S-wave is reflected, and A_1/A_0, which is independent of scaling factors at this angle, again become unity. (iv) Similar to the non-scaling case, mode conversion occurs at

two angles, but the values of the angles vary with the scaling factor l. (v) the amplitudes of reflected S-waves increase appreciably with the decrease of l.

The curves for l=2.5 in Figures 4-5 exhibit features that differ qualitatively from the other curves in the same figures, such as the intersection with curves corresponding to higher values of the dimensionless scaling parameters l. It is however noted that the plots correspond to l=2.5, a value outside the valid range of $5<l<\infty$ recommended for the second degree approximation (Granik and Ferrari, 1993), should thus be considered to be poor approximations. For such scaling ranges, use should be made of scaling approaches involving M>2, following exactly the method of analysis presented above. Still, it is of interest to retain the case l=2.5 in our study, in that different quantities are approximated with different degrees of precision for the same values of l and M. An example of this will be shown later.

The two mode conversion angles for incident P-wave are plotted in Figure 6 against the dimensionless scaling factor l. In Figure 6 and 11, the value of l is taken within the range ($5<l<\infty$) that DM theory(M=2) applies. From Figure 6, it is observed that the first critical angle of mode conversion increases sharply with l when l <30 and changes slowly when $30<l<100$, and approaches the angle 60^0 of non-scale case when l=100. The second critical angle of mode conversion decreases moderately with the increase of l and approaches the angle 77^0 of non-scale case when l=100. It is shown that the results of non-scaling case are retrieved at $l \approx 100$.

The phase changes of the reflected P-wave and S-wave with respect to that of the incident P-wave are plotted in Figures 7 and 8 against the angle of incidence with l as a parameter. The phase under consideration is defined as

$$\varphi = arctg \frac{Im(A_n/A_0)}{Re(A_n/A_0)}, \tag{47}$$

where $Im(A_n/A_0)$ indicates the imaginary component and $Re(A_n/A_0)$ the real component of A_n/A_0 with n=1 for the reflected P-wave and n=2 for the reflected S- wave.

The results of Figure 7 and Figure 8 show that: (i) For a given wavelength, the particle size, as reflected by the scaling factor, has a significant influence on the phase change. (ii) The phase change for l=100 is very close to that of l=∞, which indicates that for the value of l greater than 100, the results of DM theory are identical with those of classical theory; the phase changes for the values of l less than 100, unlike the non-scaling case where the phase difference is either 0 or π, change continuously with the incident angle and increase with the decrease of l. (iii) The reflected P-wave has abrupt phase changes of π at about 60^0 and 80^0 corresponding to the phenomenon of mode conversion of the reflected P-wave shown in Figure 4. (iv) There is no phase difference between the reflected S-wave and the incident P-wave for the non-scaling case at the whole range of incident angle; but for the scaling case, there is a phase difference between them, and the difference increases with the decrease of scaling factors l, indicating the depart from the continuum approximation assumed in classical theory. It is noted that the results corresponding to the l=2.5 are qualitatively similar to those

corresponding to larger values of l, for what pertains to the phase change diagrams.

Case IV. Reflection of incident S-wave(M=2)

For an incident S-wave, there are also a S- wave and a P- wave reflected at stress free boundary (Goodier and Bishop,1948). In this case, we assign indices n=0 to incident S wave, n=1 to the reflected P-wave and n=2 to the reflected S-wave.

By strictly following the analogous procedure of the previous sections, we obtain

$$k_0 \sin\theta_0 = k_1 \sin\theta_1 = k_2 \sin\theta_2 \tag{48}$$

$$k_0 c_T = k_1 c_l = k_2 c_T \tag{49}$$

Similarly, we can conclude from (48) and (49) that

$$k_2 = k_0, \qquad \theta_2 = \theta_0 \tag{50}$$

$$\frac{k_1}{k_0} = \frac{c_T}{c_L} = \kappa^{-1} \tag{51}$$

$$\sin\theta_1 = \kappa \sin\theta_0. \tag{52}$$

Though we will follow the same procedure to discuss the reflection of an incident S-wave, it is worthwhile to notice at this point that there are significant differences between the reflection of S- waves and P- waves. Since the velocity of propagation for the reflected P-wave is greater than that of the incident S-wave, $\kappa=c_L/c_T$ is always greater than 1; and therefore according to equation (33), the angle of the reflected S-wave is always less than that of the incident P-wave. By inspection of (52), however, the angle of the reflected P-wave is found to be always greater than that of the incident S-wave. Consequently, there will be a critical angle of incidence at which the reflection angle of P-wave equals 1/2 π. For those incident angles being greater than the critical angle, a reflected surface wave will be generated and decays exponentially with distance from the free surface. The discussion of surface waves is beyond the scope of this study. In what follows, the reflection of incident S-wave is studied, only for waves with the incident angles which do not exceed the critical angle.

By (50), (51), (52) and the stress free boundary conditions (24) and (25), the stress relation (42) for $\kappa=3^{1/2}$ can be reduced to

$$\begin{aligned}
&\left[-i\frac{9}{2}\frac{\pi}{l}\sqrt{3}\sin\theta_0+i\frac{27}{4}\frac{\pi}{l}\sqrt{3}\sin\theta_0\cos^2\theta_0\right.\\
&\left.+\frac{3}{4}\sin\theta_0\sqrt{-2+3\cos^2\theta_0}+i\frac{9}{16}\frac{\pi}{l}\sin\theta_0-i\frac{15}{16}\frac{\pi}{l}\sin\theta_0\cos^2\theta_0\right]\frac{A_1}{A_0}\\
&+\left[\frac{3}{4}\cos^2\theta_0-\frac{3}{8}+i\frac{5}{16}\frac{\pi}{l}\cos\theta_0-i\frac{5}{16}\frac{\pi}{l}\cos^3\theta_0\right]\frac{A_2}{A_0}\\
&=-\left[i\frac{1}{2}\frac{\pi}{l}\sqrt{3}\cos^3\theta_0+\frac{3}{4}\cos^2\theta_0-\frac{3}{8}-i\frac{5}{16}\frac{\pi}{l}\sqrt{3}\cos\theta_0\right]
\end{aligned} \tag{53}$$

$$
\begin{aligned}
&\left[\frac{3}{8}\sqrt{3}+i\frac{3}{16}\frac{\pi}{l}\sqrt{3(-2+3\cos^2\theta_0)}-\frac{3}{4}\sqrt{3}\cos^2\theta_0\right]\frac{A_1}{A_0} \\
&+\left[-i\frac{3}{16}\frac{\pi}{l}\sqrt{3}\sin\theta_0+\frac{3}{4}\cos\theta_0\sin\theta_0\right]\frac{A_2}{A_0} \\
&=i\frac{3}{16}\frac{\pi}{l}\sqrt{3}\sin\theta_0+\frac{3}{4}\sin\theta_0\cos\theta_0.
\end{aligned}
\tag{54}
$$

From these equations, A_1/A_0 and A_2/A_0 versus the angle of incidence with scaling factor l as a parameter are plotted in Figure 9 and Figure 10.

It is found that (i) there is a critical angle at about 35^0, which is independent of the scaling factor l and consistent with that of equation (52); (ii) at $\theta_0=0$, the reflected P- wave vanishes, the incident S- wave is reflected as a S- wave only and the magnitudes of reflected S- waves are same as that of incident S- wave for all values of l; (iii) mode conversion also occurs at two angles, as in the case of incident P- waves, at which the S-wave vanishes and incident S-wave is reflected as P-wave only; (iv) the amplitudes of reflected P-wave increase appreciably near the critical angle and reaches the maximum at the critical angle(even twice than that of incident S-wave).

For ease of viewing the dependence of the mode conversion on the microstructural variables, the two mode conversion angles versus the dimensionless scaling parameter l for an

incident S-wave are plotted in Figure 11. It is observed that both two critical angles of mode conversion increase sharply with l when l <30, vary slowly when 30<l<100, and reach a maximum value when l=100. The classical case(non-scaling) is again retrieved at l greater than 100.

By employing equation (47), with A_0 denoting the amplitude of an incident S-wave in this case, the phase changes of reflected waves to an incident S-wave for M=2 and $\kappa=3^{1/2}$ are plotted in Figure 12 and Figure 13.

It is observed that (i) phase changes of reflected waves to an incident S-wave are strongly influenced by scaling factor l. (ii) the reflected P-waves for $l \geq 100$ always have a phase difference of π with respect to that of the incident S-wave; the phase differences between the reflected P-wave and the incident S-wave for other values of l increase with the decrease of l and change continuously with the incident angle.(iii) the reflected S-waves at l greater than 100 also have a phase difference of π with respect to that of incident S-wave and have an abrupt phase change of π around 30^0~35^0, at which the mode conversion of reflected S wave occurs.

Concluding remarks

In this study, Doublet Mechanics has been used to analyze the elastic wave reflection at granular material-free space interfaces. The amplitude ratios of reflected waves to incident

waves and phase shifts of the reflected waves have been obtained analytically. It was found that the results of first order approximation, which corresponds to the situation of non-scaling, isotropic granular media, are consistent with those obtained using classical continuum theory.

Upon accounting for scaling effects, novel results were established, that have no counterpart in classical elastodynamics. In particular, it was found that the critical angle of mode conversion, the amplitude ratios, and the phase shifts in reflection phenomena are dependent on a dimensionless scaling parameter. Such dependence is more pronounced at shorter dimensionless wavelength, that is for larger granule sizes for a fixed wavelength, where the continuum assumption of classical elastodynamics is no longer valid. The non-dimensionality of the scaling parameter renders the present results applicable to materials with significantly different typical microstructural dimensions, as long as the wavelengths are proportionately scaled. The classical elastodynamic reflection results were found to hold as an excellent approximation in the for wavelength-to-granule size ratio of order 100.

References

Achenbach, J.D. (1973) *Wave propagation in elastic solids*, North-Holland Publishing Company.

Goodier and Bishop (1951) A Note on critical reflection of elastic waves at Free surfaces. *J.*

of Applied Physics. **23**, 124-126.

Kolsky, H. (1963) *Stress waves in solids*. Dover, New York.

Granik, V.T. and Ferrari, M. (1993) Microstructural mechanics of granular media. *Mech. Mater.* **15**, 301-322.

Granik, V.T. and Ferrari, M. (1995) Advances in Doublet Mechanics I: Multi-scale elastic wave propagation. *Report No. UCB/SEMM-95/03*, Department of Civil Engineering, University of California, Berkeley (also, submitted for publication, Journal of Mechanics and Physics of Solids)

Figure 1. Reflection of an incident P-wave at the interface of granular medium and free space with a sketch of corresponding doublet orientation (τ_3 parallel to x_1 axis); θ_0 - the incident angle of the incident P-wave; θ_1 - the reflection angle of the reflected P-wave; θ_2 - the reflection angle of the reflected S-wave; ϕ - the angle between the directions of two doublets.

Figure 2. Amplitude ratios of the reflected waves to the incident wave for an incident P-wave in the non-scaling case of M=1. A_0 - the amplitude of the incident P-wave; A_1 - the amplitude of the reflected P-wave; A_2 - the amplitude of the reflected S-wave.

Figure 3. Reflection of an incident P-wave at the interface of granular medium and free space with the sketch of corresponding doublet orientation (τ_3 in an angle of γ with respect to x_1 axis); θ_0 - the incident angle of the incident P-wave; θ_1 - the reflection angle of the reflected P-wave; θ_2 - the reflection angle of the reflected S-wave.

Figure 4. Real components of amplitude ratios of the reflected P-wave to the incident P-wave in the scaling case of M=2 with l, the dimensionless scaling factor as a parameter.

Figure 5. Real components of amplitude ratios of the reflected S-wave to the incident P-wave in the scaling case of M=2 with l, the dimensionless scaling factor as a parameter.

Figure 6. Two mode conversion angles for an incident P-wave versus the dimensionless

scaling factor l; —— the first mode conversion angle, ----- the second mode conversion angle.

Figure 7. Phase changes of the reflected P-wave with respect to the incident P-wave in the scaling case of M=2 with l, the dimensionless scaling factor as a parameter

Figure 8. Phase changes of the reflected S-wave with respect to the incident P-wave in the scaling case of M=2 with l, the dimensionless scaling factor as a parameter.

Figure 9. Real components of amplitude ratios of the reflected P-wave to the incident S-wave in the scaling case of M=2 with l, the dimensionless scaling factor as a parameter.

Figure 10. Real components of amplitude ratios of the reflected S-wave to the incident S-wave in the scaling case of M=2 with l, the dimensionless scaling factor as a parameter.

Figure 11. Two mode conversion angles for an incident S-wave versus the dimensionless scaling factor l; —— the first mode conversion angle, ----- the second mode conversion angle.

Figure 12. Phase changes of the reflected P-wave with respect to the incident S-wave in the scaling case of M=2 with l, the dimensionless scaling factor as a parameter.

Figure 13. Phase changes of the reflected S-wave with respect to the incident S-wave in the scaling case of M=2 with l, the dimensionless scaling factor as a parameter.

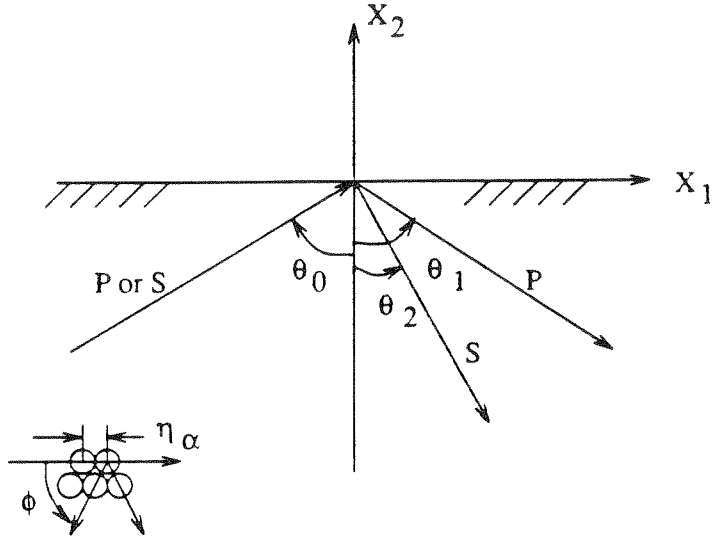

Figure 1

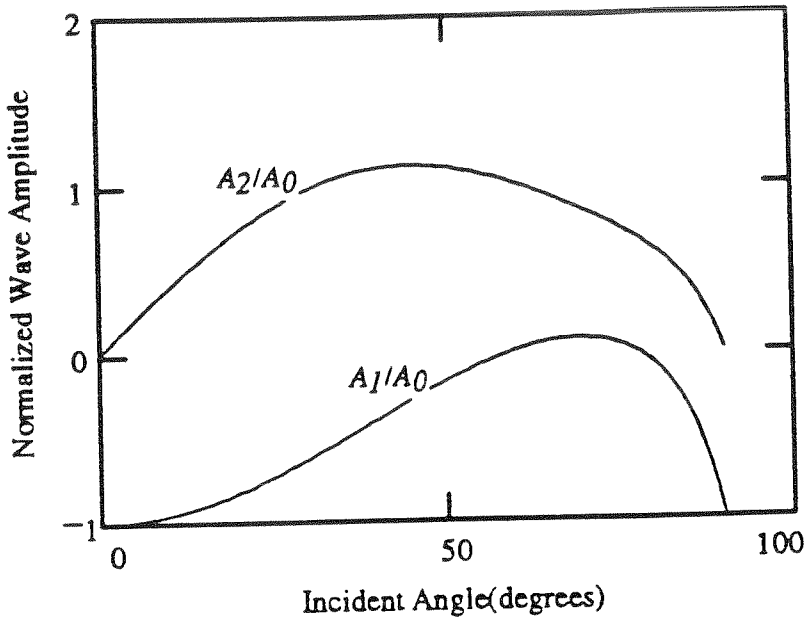
2
1
0
−1
0
50
100
Normalized Wave Amplitude
Incident Angle(degrees)
A_2/A_0
A_1/A_0

Figure2

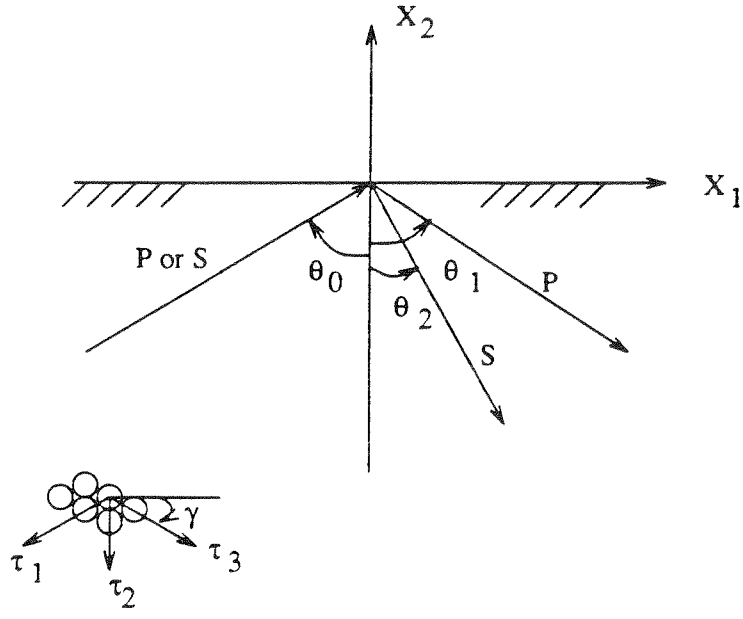

Figure 3

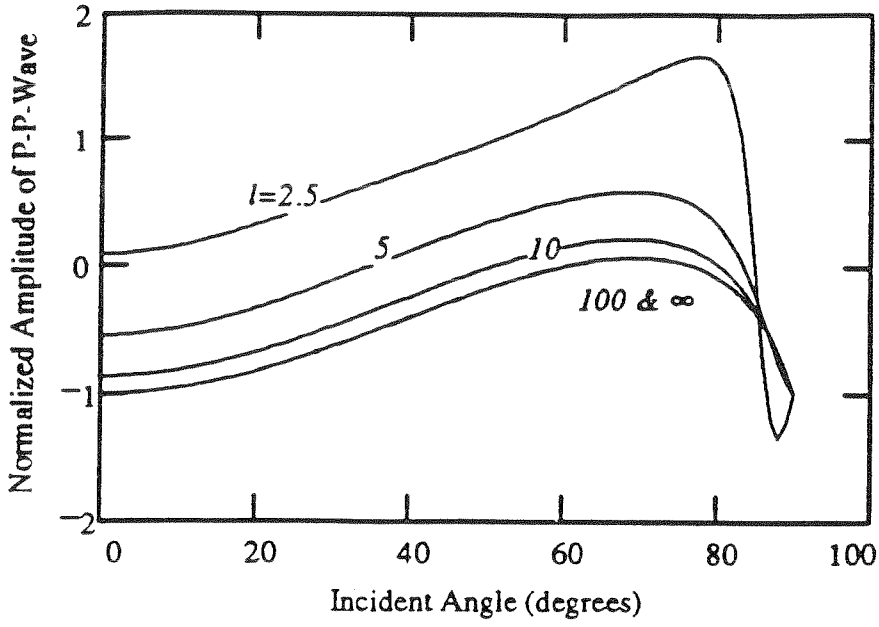
Normalized Amplitude of P-P-Wave
2
1
0
−1
−2
0
20
40
60
80
100
Incident Angle (degrees)
l=2.5
5
10
100 & ∞

Figure4

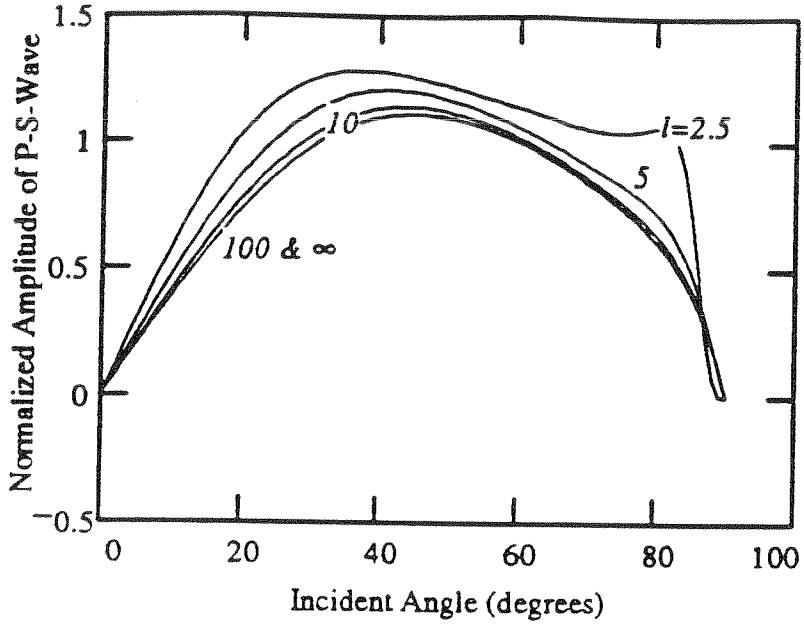
Normalized Amplitude of P-S-Wave
1.5
1
0.5
0
−0.5
0
20
40
60
80
100
Incident Angle (degrees)
l=2.5
10
5
100 & ∞

Figure5

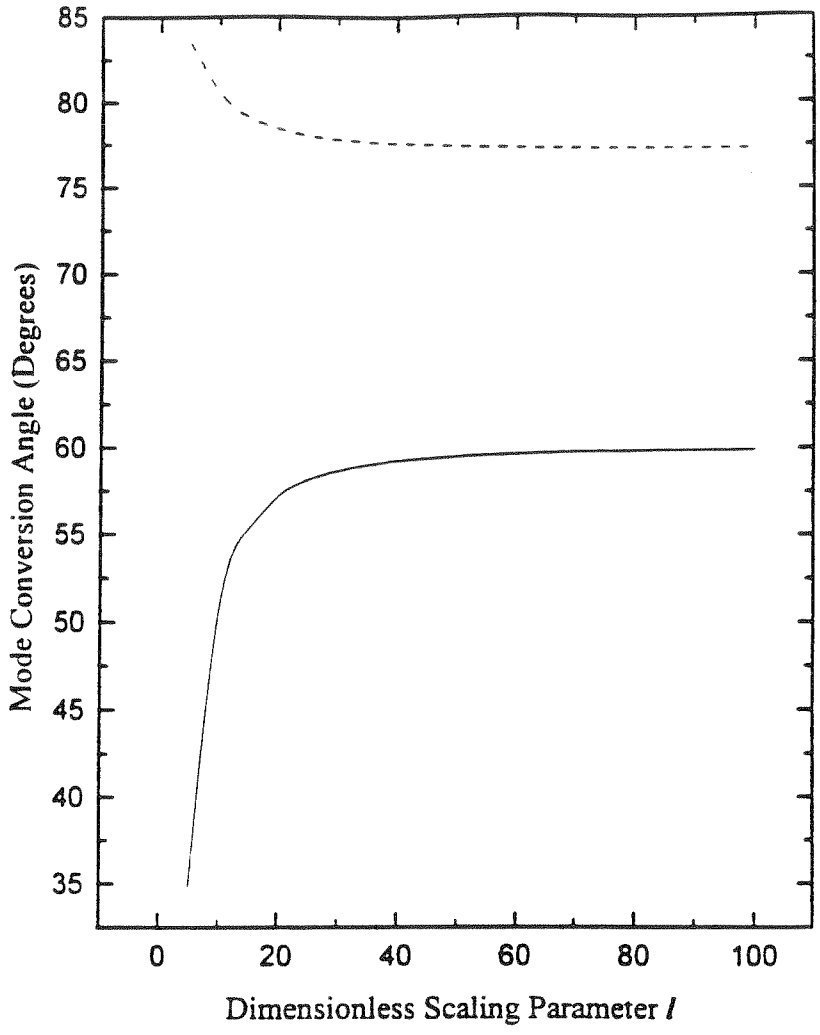
85
80
75
70
65
60
55
50
45
40
35
Mode Conversion Angle (Degrees)
0
20
40
60
80
100
Dimensionless Scaling Parameter *l*

Figure 6

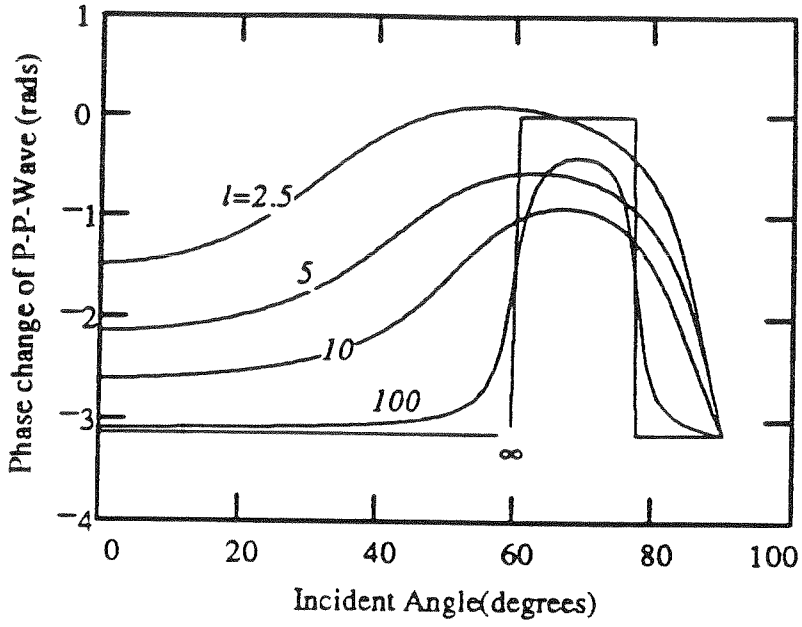
Phase change of P-P-Wave (rads)
1
0
−1
−2
−3
−4
l=2.5
5
10
100
∞
0
20
40
60
80
100
Incident Angle(degrees)

Figure7

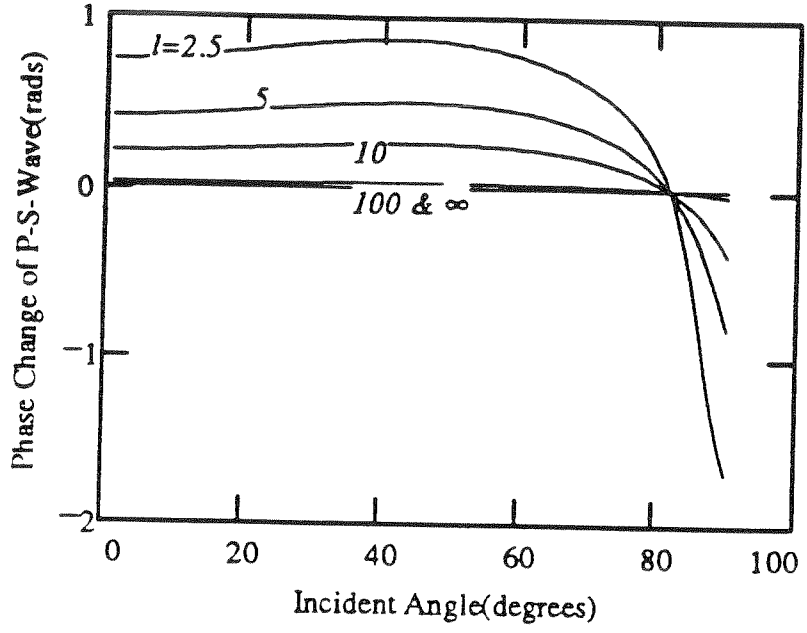
1
0
−1
−2
l=2.5
5
10
100 & ∞
0
20
40
60
80
100
Phase Change of P-S-Wave(rads)
Incident Angle(degrees)

Figure8

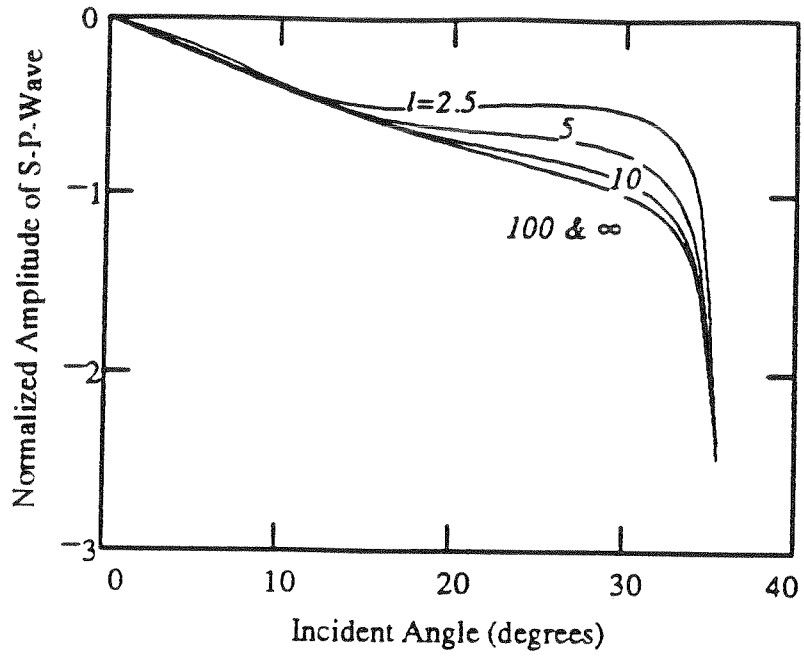
0
−1
−2
−3
Normalized Amplitude of S-P-Wave
l=2.5
5
10
100 & ∞
0
10
20
30
40
Incident Angle (degrees)

Figure9

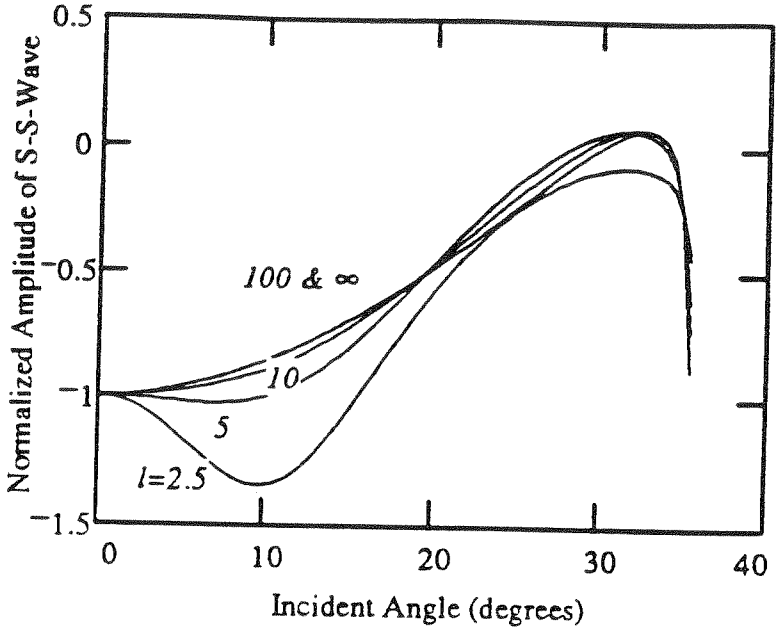
0.5
0
−0.5
−1
−1.5
Normalized Amplitude of S-S-Wave
100 & ∞
10
5
l=2.5
0
10
20
30
40
Incident Angle (degrees)

Figure10

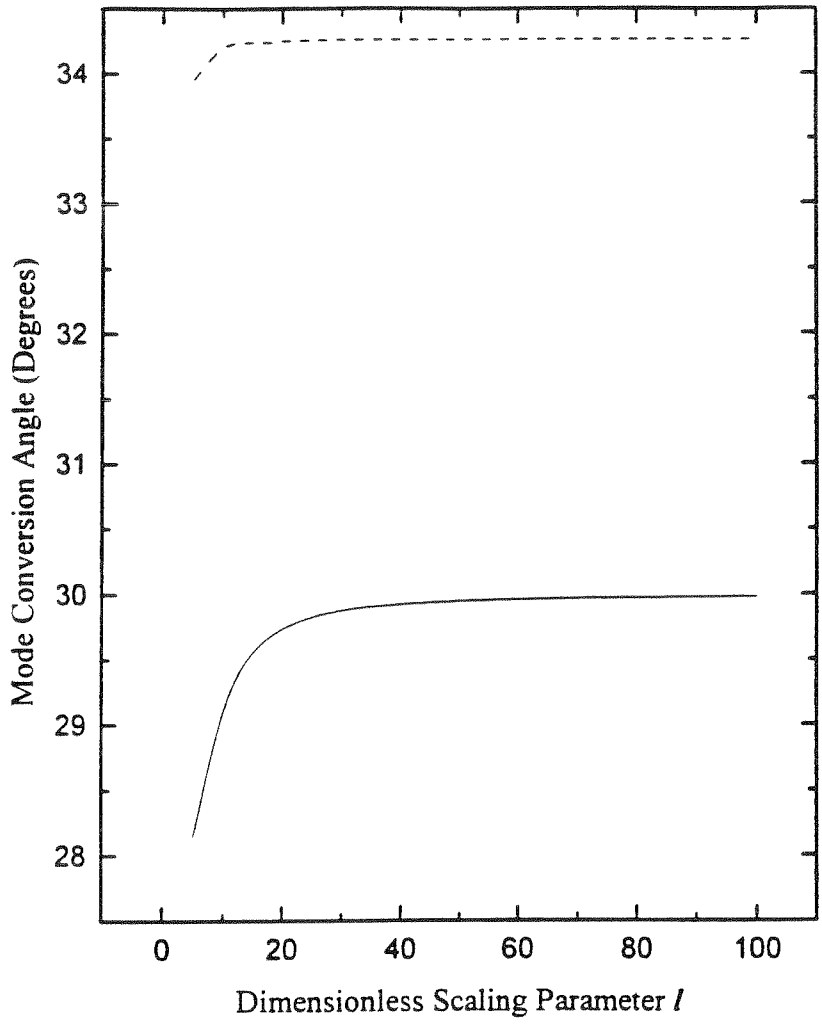
Mode Conversion Angle (Degrees)
34
33
32
31
30
29
28
0
20
40
60
80
100
Dimensionless Scaling Parameter l

Figure 11

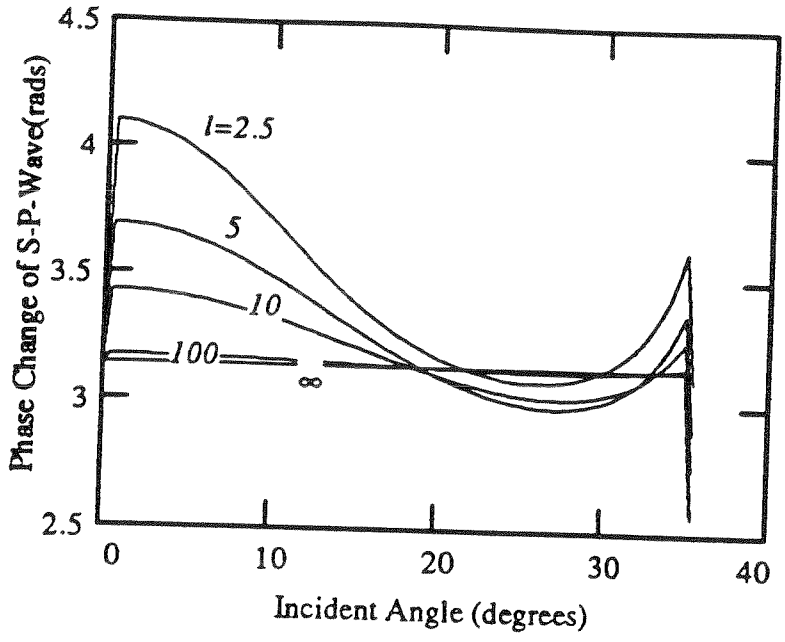
4.5
4
3.5
3
2.5
Phase Change of S-P-Wave(rads)
l=2.5
5
10
100
∞
0
10
20
30
40
Incident Angle (degrees)

Figure12

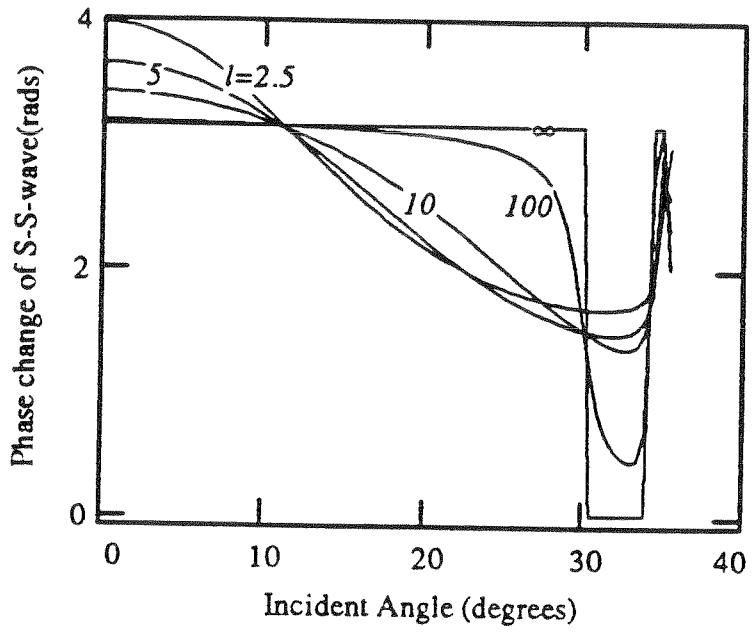
4
2
0
0
10
20
30
40
Phase change of S-S-wave(rads)
Incident Angle (degrees)
5
l=2.5
10
100
∞

Figure13